Femtosecond laser-based fabrication of a new model material to study fracture

A. Weck, T.H.R. Crawford, A. Borowiec, D.S. Wilkinson, J.S. Preston

May 13, 2008

A. Weck
McMaster University, Department of Materials Science and Engineering. 1280 Main Street West, Hamilton, ON, Canada. weckag@mcmaster.ca
T.H.R. Crawford
Department of Engineering Physics, McMaster University, Hamilton, Ontario, Canada, L8S 4L7.
A. Borowiec
Department of Engineering Physics, McMaster University, Hamilton, Ontario, Canada, L8S 4L7.
D. Wilkinson
McMaster University, Department of Materials Science and Engineering. 1280 Main Street West, Hamilton, ON, Canada.
J.S. Preston
Department of Engineering Physics, McMaster University, Hamilton, Ontario, Canada, L8S 4L7.

Abstract

The ductile fracture process consists of the nucleation, growth and coalescence of voids in a material. Predictive models of ductility require a complete understanding of the coalescence event. However, coalescence occurs over very small strains and is therefore difficult to observe experimentally. We have addressed this by developing a new class of model material. It consists of femtosecond laser drilled holes and diffusion bonded metallic sheets, which can be mechanically tested in situ either by scanning electron microscopy (SEM) or by X-Ray Computed Tomography (XRCT). The fabrication steps are presented and the model material is characterized by optical and electron microscopy, nanoindentation and tomography. The heat affected zone around the laser holes is found to be harder than the unaffected material and consists of nano-scale grains. Finally we show that the coalescence event is well captured using both SEM and XRCT. The fabrication method is adaptable to a wide range of materials and enables one to produce 2D and 3D arrays of holes or cracks with controlled size, volume fraction and distribution.

PACS 62.20.Mk;62.25.+g;79.20.Ds

1 Introduction

Ductile fracture of metals involves a sequence of overlapping processes that includes the nucleation, growth and coalescence of voids. Of these, coalescence is of vital importance because it dictates the ductility of the metals. It is however the least understood. As coalescence is a stochastic event occurring over relatively short elongations, it is rather difficult to capture experimentally. Sound experimental data are therefore required to fully characterize the parameters governing this coalescence event. The main parameters affecting coalescence include: (a) the geometry (void size, shape, orientation, spacing) (b) the material properties (work hardening rate, strain rate sensitivity) and (c) the stress state (stress triaxiality) ([22], [6], [19], [10], [20], [11], [2]). The aim is to be able to experimentally vary these parameters to evaluate their respective influences. Commercially available materials have complicated microstructure (random size, shape and distribution of inhomogeneities) which is difficult to analyze and one needs to use instead model materials with controlled microstructure in order to un-

derstand the basics of the coalescence event. Attempts to fabricate such model materials for the study of the ductile fracture processes have already been made. Babout et al. [1] and Gammage et al. [10] for example fabricated metal matrix composites made of an aluminum matrix reinforced by zirconia and alumina spheres respectively. These model materials are useful to study damage nucleation events but are of limited value when one wants to study the coalescence event in detail, because the void density is still stochastically controlled and the nucleation varies with strain. Magnusen et al. [15], Jia et al. [12] and Nagaki et al. [17] fabricated model materials by drilling holes through metallic sheets. They used hole diameters of 1.2 mm, 1 mm and 0.8 mm respectively. This simplifies the microstructure because of the limited number of holes and their more or less controlled positioning and removes the nucleation problem. However, these model materials contain larger holes than those found in real materials, where the void sizes are ranging from 0.001 to 0.05 mm ([16]). Furthermore, they lack the constraint found in real materials because the holes run through the sheets, i.e. it is a strictly 2D study. In real materials the holes are in the bulk, thus a 3D approach is required. If one could eliminate nucleation events, produce a simple controlled microstructure, and use the constraint and void sizes found in real materials, it would greatly simplify the analysis of the growth and coalescence of voids. The present work describes the fabrication and characterization of two new model materials for ductile fracture studies that meet most of these requirements. The first consists of a controlled two dimensional array of fine laser-drilled holes in metallic sheets (2D approach) to be pulled in situ in a scanning electron microscope (SEM) (figure 1(a)). The second consists of bulk samples with embedded holes. To fabricate it the sheets with laser-drilled holes are diffusion bonded together to form the 3D array of holes (figure 1(b,c)). The first part of this paper deals with the selection of six different materials that are used to build and characterize the model materials, namely copper, titanium, Glidcop (copper with fine dispersion of alumina particles), commercial purity aluminum, aluminum alloy 5052 and stainless steel. We then describe the fabrication of the two types of model materials. Finally, the samples are characterized by SEM, transmission electron microscopy (TEM), nanoindentation and x-ray computed tomography (XRCT) to see whether they are suitable for ductile fracture studies.

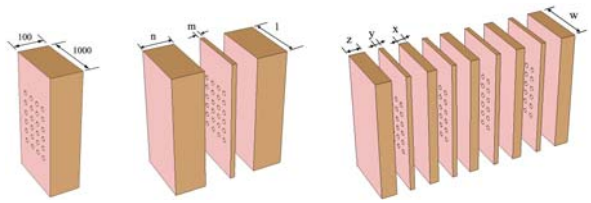

(a) (b) (c)

Figure 1: (a) Schematic Drawing of the 2D material (dimensions in microns), and exploded drawings of the 3D material with (b) one and (c) multiple sheets with holes. Dimensions are in microns. The value of the letters l,m,n and w,x,y,z depends on the resolution of the tomography set-up used and the chosen hole spacing.

2 Materials Selection

The materials were chosen based on various parameters such as ductility, crystal structure, grain size, strain rate sensitivity and extent of the laser induced heat affected zone. As holes can be laser drilled in virtually all materials, this is not an issue so far for the material selection. Pure copper (99.999%) and commercial purity aluminum (99.99%) are used as reference materials as they have good ductility that will allow one to follow the coalescence event over significant deformations. Commercial purity titanium (99.7%) is used to show the effect of the crystal structure (hcp) on hole deformation and coalescence compared to fcc materials (copper, glidcop, aluminum). In order to limit grain growth during diffusion bonding and therefore have more grains in the cross section of the samples, an oxide dispersion strengthened copper named Glidcop-Al25 is also used. This material consists of a copper matrix containing 0.25% by wt. of aluminum in the form of a fine dispersion (50 nm in diameter) of alumina oxides (Al_2O_3). The particles inhibit grain growth even at high temperatures and increase the strength of the material. The aluminum alloy 5052 is chosen for its negative strain rate sensitivity. Finally, to check whether the heat affected zone induced by the laser drilling is different for various materials, aluminum, copper and stainless steel are chosen for their different combi-

nations of heat capacity and heat conductivity properties.

3 Fabrication of the model material

The remaining parameters to be selected are the size of the holes, their spacing and their distribution for the different materials previously described. If one wants to reproduce the microstructural features found in real materials, hole sizes in the range of a few microns to tens of microns should be selected. However, the hole dimensions must also be compatible with the techniques used to characterize them. The 2D experiments are carried out in an SEM with a resolution of about 10 nm. However, the resolution attainable using X-Ray tomography, expressed in terms of voxel size, depends on the system used and varies in this study from 0.5 to 2 μm. (Current lab-based XRCT systems now offer comparable resolution in absorption mode). We require that the initial hole diameter be at least 20 times the voxel size. Table 1 shows the selected hole sizes as a function of the tomography system used in this study. Once the hole diameter is chosen, a suitable volume or area fraction of holes must be chosen. This can be selected freely according to the model one wants to test. Similar freedom exists in terms of hole distribution and hole shape.

Table 1: Hole size for a given resolution of the tomography set-up

Tomography set-up	Resolution	Hole size
ESRF-Beamline ID19	1.9 μm	40 μm
Spring-8 Beamline BL020XU	0.48 μm	10 μm
ESRF-Beamline ID15	1.6 μm	40 μm

3.1 Laser hole drilling

Prior to laser drilling, the sheets are polished using a 1 μm diamond suspension providing a measured average roughness of about 0.1 μm. For the 2D experiments, single sheets 100 μm in thickness are used. For the 3D experiments, the sheets are stacked together as in figure 1(b,c) and welded on one end using a spot welding machine. The holes are then drilled in the sheets by flipping each sheet over like the pages of a book. This ensures good positioning of a given array of holes with respect to the arrays on the other sheets. On top of the last sheet, lines are drawn with the laser for subsequent reference when milling dog bone shaped samples out of the bonded stack. To drill the holes, a femtosecond laser is chosen because it allows the drilling of micron-size holes ([27])and has been shown to provide holes with a clean finish ([8]). Additionally, femtosecond lasers typically produce a relatively small heat affected zone (HAZ) compared to holes drilled with lasers of longer pulse lengths ([13]). The laser set-up, which includes a vacuum chamber placed on a translation stage, is described elsewhere ([5]). Several parameters can be varied namely: environment (vacuum, air), pulse energy, number of pulses per hole, polarization (linear polarization, circular polarization and rotating polarization obtained with a spinning half wave plate) and spot size (depending on the lens or objectives used to focus the laser beam). Wynne and Stuart [26] showed that for high aspect ratio holes a faster material removal rate is obtained in vacuum (relevant for the case of our 2D approach in which the aspect ratio of the holes is $\sim$10). However, when a large number of holes per sheet have to be drilled, ablated material can be deposited on the chamber window. Samples were therefore drilled in air because it greatly reduces material deposition on the vacuum chamber window. Note however that the sample is still placed in a stainless steel vacuum chamber (without vacuum pump turned on) to attenuate emitted X-Rays that could be harmful to the operator as shown by Thøgersen et al [21]. The vacuum chamber is placed on a translation stage for precise positioning of the holes (resolution 0.1 μm). Any array of holes can then be accurately drilled to study the influence of the geometry on coalescence. For the 10 and 40 μm in diameter holes, a pulse energy of 10 and 17 μJ respectively and 1000 pulses per hole are used as they give the best compromise between drilling time and hole shape. A hole diameter of 10 μm is obtained using a 5$\times$ objective and that of 40 μm using a plano-convex lens with a focal length of 75 mm. The spinning half wave plate is chosen for all experiments as it was shown by Nolte et al. [18] to provide best hole shape, especially on the exit side.

3.2 Diffusion bonding

After laser drilling, the stack of sheets is placed in an ultrasonic bath for 15 minutes and then chemically etched to remove the oxide layer. The copper and Glidcop samples were chemically polished using a solution of 20% sulfuric acid in water. The titanium samples were not chemically polished as it was observed that titanium dissolves its own oxide at temperatures higher than 950°C. All diffusion bonding experiments took place in a reducing atmosphere made of a mixture of 4% hydrogen in argon. The samples are finally diffusion bonded using the parameters shown in table 2. Surface preparation is critical for diffusion bonding, however with appropriate care we were able to attain excellent bond strength.

Table 2: Diffusion bonding parameters

Material	Temperature (°C)	Pressure (MPa)	Time (min)	Environment
Copper	920	3	40	4%H_2 in Ar
Glidcop	1000	3	30	4%H_2 in Ar
Titanium	960	3	60	4%H_2 in Ar

4 Model material characterization

To verify that our model materials can be used to represent the behavior of real materials, they are characterized using several methods. The position, shape and heat affected zone of the laser drilled holes are first characterized. Then the microstructure of the diffusion bonded materials is observed. Finally, mechanical testing is performed to verify the bonding of the sheets in the 3D approach.

4.1 Laser hole characterization

Figure 2(a) is an SEM micrograph of a 100 μm thick aluminum sheet after femtosecond laser hole drilling of a rectangular array rotated at 45 degrees to the vertical. It can be seen that the holes are precisely spaced and that their shape is circular. The cross section of the holes has been observed under an optical microscope, presented in figure 2(b). Such a sample is obtained using a microtome with a diamond knife. In figure 2(b) the laser beam entered the sample from the top of the picture and exited

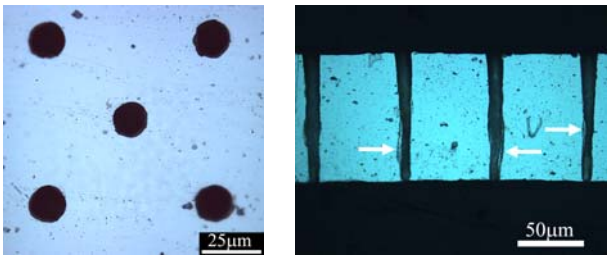

(a) (b)

Figure 2: Optical image of (a) a regular array of femtosecond laser drilled holes and (b) the cross section of an array of laser drilled holes.

at the bottom. The entrance size (10 μm) of the hole is larger than its exit size (8 μm) because as the laser goes through the sample, it interacts with the sides of the hole. Even though a femtosecond laser has been chosen to drill the holes, there is still some evidence of a remelted layer as shown by the white arrows in figure 2(b). The non-uniformity of this layer has already been observed by Luft et al. [14]. To further study the redeposited layer, TEM samples were prepared using a microtome. It allowed us to cut a TEM sample from the side of a hole drilled in a high purity aluminum foil. A dark field TEM picture is shown in figure 3(a) where, from left to right, we see the laser hole then the HAZ and finally the unaffected material. The thickness of the HAZ varies from about 300 nm to 2 μm. Figure 3(a) shows that the grains in the HAZ have a size ranging from a few to tens of nanometers. Figure 3(b) represent the diffraction pattern from the unaffected region (right side of figure 3(a)) and figure 3(c)from the nano-grains region (left side of figure 3(a)). The ring pattern in figure 3(c) confirm the presence of nano gains in this region.

It has also been shown that drilling with a femtosecond laser can lead to the formation of internal stresses due to the solidification of the remelted layer and/or the pressure induced by the laser ([3], [14]). In order to know more about the mechanical properties of the HAZ, nanoindentation experiments have been carried out on a NanoindenterII to measure the hardness around the holes. These experiments have been done on commercial purity aluminum (99.99%), aluminum alloy 5052 and stainless steel. The samples have been carefully polished with a

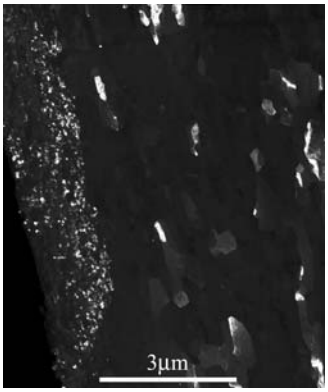

(a)

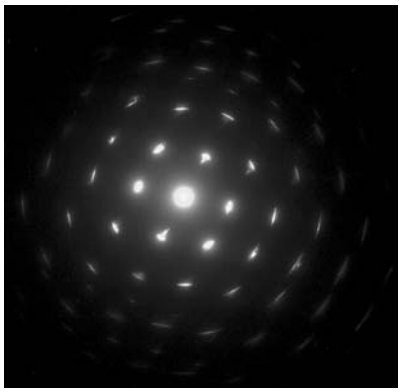

(b)

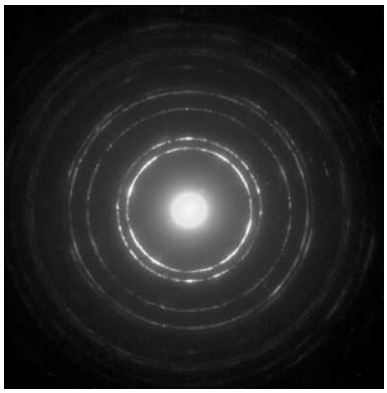

(c)

Figure 3: (a) TEM image of the side of one hole with from left to right the laser hole, the resolidified layer and the unaffected material. (b) Diffraction pattern from the unaffected area and (c) from the affected region showing rings characteristic of the presence of nano-grains

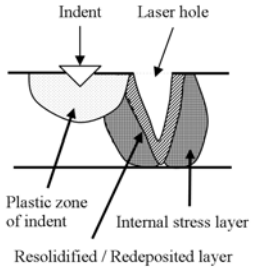

(a)

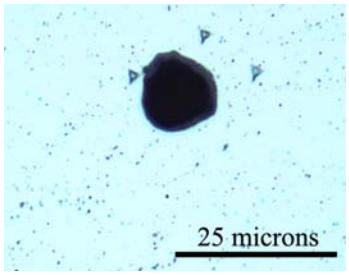

(b)

Figure 4: (a) Schematic illustration of the indentation close to a laser drilled hole and (b) an optical micrograph of 3 indents placed around a hole in commercial purity aluminum.

0.05 μm alumina suspension to reduce the size of the oxide layer and the polishing damaged layer. A load of 2N is chosen for the aluminum and 5 N for the stainless steel in order to have an indent width of about 2 μm for all the materials. This leads to an indented depth of about 300 nm, which is deep enough to avoid measurement artifacts coming from the thin (10 nm) oxide layer on the sample surface. When the indent penetrates the samples, it creates a deformed region with a high dislocation density called the "plastic zone" whose size is approximately 3 times the diameter of the indent. Therefore, the indents are placed at a distance of $\sim$3 μm from the edge of the laser drilled holes in order to have the plastic zone just reaching the edge of the hole (figure 4(a)). About 20 indents are made per material. In figure 5 the indents probing the HAZ are labelled "close to hole" and the reference indents placed away from the holes are called "Matrix". The results are similar for different materials and show that the material is harder close to the holes than away from the holes. The increased strength associated with a layer surrounding each hole is clearly detrimental for the study of ductile fracture since such effects are not present in real materials containing holes. In order to reduce the effect of the HAZ, samples have been annealed after the laser drilling and indentation tests were then carried out as described above. The annealing temperature was 400°C for the aluminum samples and 900°C for the stainless steel samples. Within experimental scatter the results show that after annealing the hardness close to the hole is the same as that in the unaffected material.

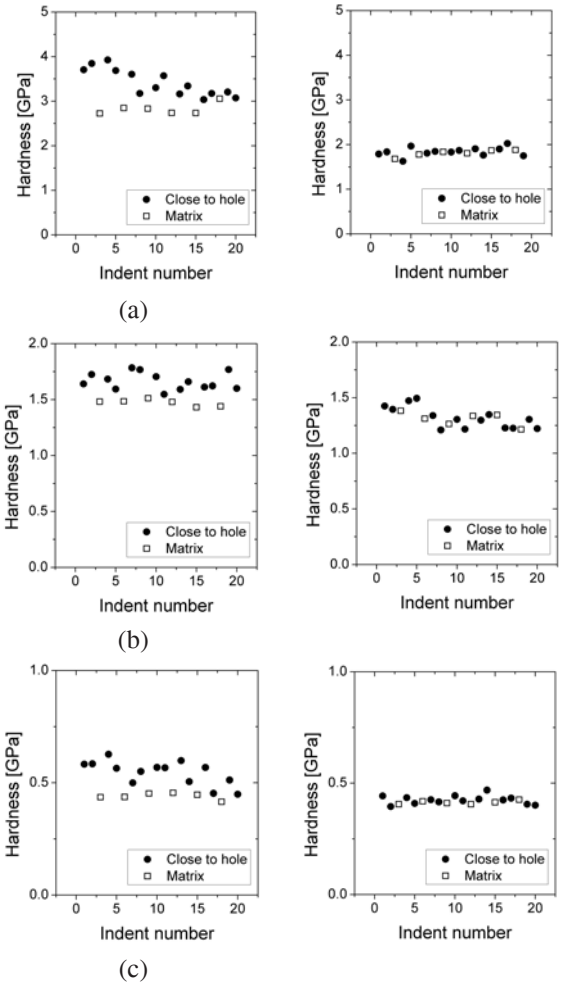

Figure 5: Nano-indentation results for indents placed close to holes and away from them ("Matrix") before (left) and after (right) heat treatments on 3 different materials: (a) stainless steel (b) aluminum alloy 5052 and (c) commercial purity aluminum.

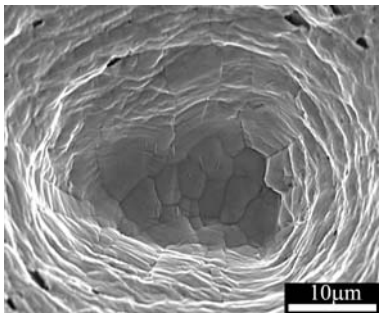

Figure 6: SEM image of the fracture surface of a Glidcop sample containing one sheet of holes diffusion bonded between two other Glidcop hole free sheets. The hole was drilled from right to left on the image and grain growth can be observed in the middle.

The relatively large scatter in hardness close to the holes can be explained by the fact that the indent position varies with respect to the edge of the hole (figure 4(b)). This leads to variability in the amount of plastic zone that is within the heat affected zone. These hardness results are therefore only qualitative. However, there is a clear and significant difference in the results before and after annealing. It is still not clear what causes the decrease in hardness following annealing. However, three explanations are proposed: the first is that laser drilling generates high dislocation densities around the hole [4] and these are recovered by annealing. The second explanation is that nano-scale grains undergo recrystallization or grain growth during annealing. Figure 6 shows a hole from the fractured surface of a Glidcop sample. Grain growth can be observed in the middle of the hole, confirming the hypothesis of grain growth in the HAZ. Finally, internal stresses generated by the laser drilling [3], which increase the measured hardness, are relieved during annealing.

4.2 Microstructure characterization

During the diffusion bonding process, we see substantial recrystallization and grain growth for the copper samples and grain growth for the titanium samples (prior to bonding the copper was in a cold rolled state and the grain size of the titanium was 5 μm). Figure 7(a) shows an optical micrograph of a copper sample containing 3 diffu-

sion bonded sheets. The grain size is large ranging from 100 to 500 μm. Figure 7(b) shows the cross section in a stack of 28 diffusion bonded titanium sheets with a final grain size of about 50 μm. The Glidcop samples are chosen in part because of their resistance to grain growth. This is confirmed in figure 7(c) where the grain size of a Glidcop sample containing two diffusion-bonded sheets is 10 μm in the rolling direction and 2 μm in the transverse direction. One can see that in the case of copper, the oxide layer prevents the grains from growing through the boundary between the sheets. The contrary occurs in the titanium sample for which the grain size is bigger than the layer thickness because titanium dissolves its own oxide at temperatures greater than 950°C. In order to check whether the holes still have the same shape and spacing after the diffusion bonding process, 3D images were obtained using X-Ray imaging. High resolution tomographic experiments were performed using synchrotron X-ray sources on beamline ID19 and ID15 at the European Synchrotron Radiation Facility (ESRF) in France and on beamline BL020XU at the Japanese Super Photon Ring (SPRing-8). A description of the tomography setups can be found elsewhere ([7], [24]). Figure 8 shows a reconstruction of the tomography data with transparency applied to the matrix in order to see the holes. The tomography results show that the array of holes is very regular and that the initial hole shape is preserved after diffusion bonding. The materials fabricated in this study are suitable for X-Ray computed tomography experiments as the absorption contrast between the holes and the material is rather strong. Also, we conclude that the bonding is good as no contrast due to debonding is observed.

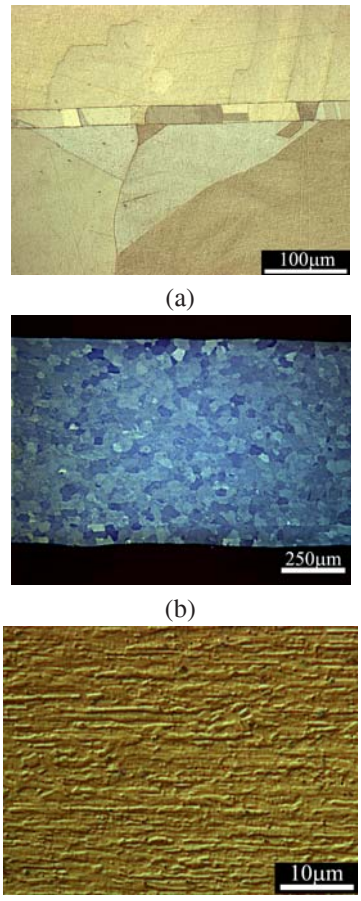

(a)

(b)

(c)

Figure 7: Optical micrographs showing the grain size after diffusion bonding in (a) copper, (b) Glidcop and (c) titanium.

4.3 Mechanical testing

Tensile tests have been carried out on an Instron screw driven tensile testing apparatus at a speed of 1 mm/min. The tensile tests were performed on a copper and Glidcop sample containing one sheet with laser drilled holes corresponding to the situation represented in figure 1(b). The fractured surfaces are then observed in an SEM to look for eventual debonding of the sheets. Figure 9 shows SEM micrographs of the fracture surface of copper and Glidcop samples. In both cases, there is no visible evidence of debonding between the sheets. Tensile tests were also carried out in-situ in a scanning electron microscope and

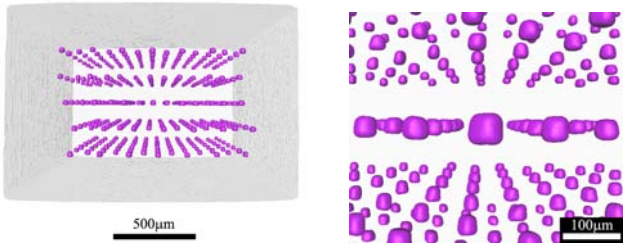

(a) (b)

Figure 8: (a) 3D tomographic reconstruction of the holes in a titanium sample and (b) close up on the holes.

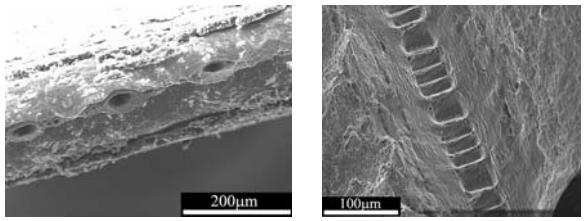

(a) (b)

Figure 9: SEM image of the fracture surface of the copper (a) and Glidcop (b) samples containing one sheet of laser drilled holes

in an X-Ray Computed Tomography set-up. The results shown in figure 10(a) represent the holes at the point of coalescence for a three layer copper sample with holes in the embedded layer (situation from figure 1(b)) and tested at SPRing-8. The results in figure 10(b) are from an SEM in-situ tensile test on a 5052 aluminum alloy and correspond to the case in figure 1(a). Again, the coalescence event is well captured.

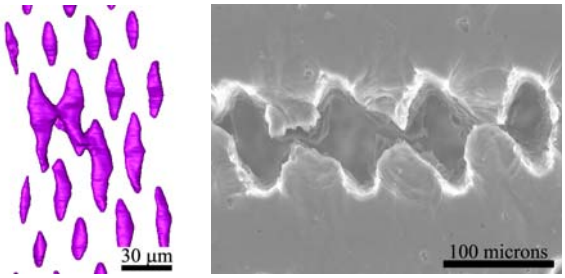

(a) (b)

Figure 10: (a) 3D tomographic reconstruction of the holes in a copper sample and (b) SEM image during in-situ tensile test on aluminum alloy 5052. Both images where taken at the coalescence event.

5 Conclusion and potential applications

A new model material has been developed to give insight into the ductile fracture process and especially the coalescence event. The fabrication process consists of drilling holes in metallic sheets using a femtosecond laser followed by diffusion bonding. The result is a 3D array of holes in the bulk of a metallic sample. The microstructure of the model material has been characterized and also its mechanical properties. It is shown that this model material is suitable for in-situ ductile fracture studies using either an SEM or X-Ray computed tomography. A variety of model materials with different microstructures and mechanical properties can be fabricated. Large grains are obtained in copper, medium sized grains in titanium and small grains in Glidcop. Also materials with different crystal structure (hcp for titanium versus fcc for copper) and different strength (copper versus Glidcop) can be prepared. It has been shown that even though there is a heat affected zone around the laser drilled hole, it can be transformed by annealing to have the same mechanical properties as the unaffected material. Any pre-designed array of laser drilled holes can be obtained and the diameter of the hole can be controlled and adjusted to fit the resolution limitations of the X-Ray tomography (see figure 1).

Many applications of this model material are possible. It has already been demonstrated ([25]) using these model materials that the hole growth and coalescence is different in the 2D and 3D approaches due to constraining effect in the 3D case. One could also for instance easily reproduce a regular array of holes to test the numerous fracture models in the literature relying on uniform void distribution in a material. ([23], [11], [20]). For example, Cox and Low [9] showed that a second population of voids between larger voids reduces significantly the amount of deformation that can be applied to a material before it fractures. This effect can be studied experimentally by drilling holes with different diameter (either by defocusing the laser beam or using lenses with different focal length) to simulate the presence of two populations of voids in a material. Another application is in the field of fracture mechanics, where the behaviour of cracks is studied. By translating the sample while drilling, a shape resembling a crack can be formed. One can then for instance drill holes in front of this crack to study the void growth and coalescence ahead of a crack. This situation has already been modelled by several authors. Finally, because the position of the holes can be precisely monitored, one could drill holes on grain boundaries, twin boundaries, etc. to study the growth of voids in specific locations in the material.

Acknowledgement

We gratefully acknowledge the support of the Canada Foundation for Innovation (CFI) and the Ontario Innovation Trust (OIT) for infrastructure and the Natural Sciences and Engineering Research Council of Canada (NSERC). Also, we thank N. Braidy for assistance with the TEM.

References

[1] L. Babout, E. Maire, J.Y. Buffire, and R. Fougres. Characterization by x-ray computed tomography of decohesion, porosity growth and coalescence in model metal matrix composites. *Acta Materialia*, 49(11):2055–2063, 2001.

[2] A. A. Benzerga. Micromechanics of coalescence in ductile fracture. *Journal of the Mechanics and Physics of Solids*, 50(6):1331–1362, 2002.

[3] A. Borowiec, D. M. Bruce, D. T. Cassidy, and H. K. Haugen. Imaging the strain fields resulting from laser micromachining of semiconductors. *Applied Physics Letters*, 83(2):225–227, 2003.

[4] A. Borowiec, M. Couillard, G. A. Botton, and H. K. Haugen. Sub-surface damage in indium phosphide caused by micromachining of grooves with femtosecond and nanosecond laser pulses. *Applied Physics A-Materials Science and Processing*, 79(8):1887–1890, 2004.

[5] A. Borowiec and H.K. Haugen. Femtosecond laser micromachining of grooves in indium phosphide. *Applied Physics A: Materials Science and Processing*, 79(3):521–529, 2004.

[6] D. Broek. The role of inclusions in ductile fracture and fracture toughness. *Engineering Fracture Mechanics*, 5(1):55–56, 1973.

[7] J.-Y. Buffire, E. Maire, P. Cloetens, G. Lormand, and R. Fougres. Characterization of internal damage in a mmcp using x-ray synchrotron phase contrast microtomography. *Acta Materialia*, 47(5):1613–1625, 1999.

[8] B. N. Chichkov, C. Momma, S. Nolte, F. von Alvensleben, and A. Tünnermann. Femtosecond, picosecond and nanosecond laser ablation of solids. *Applied Physics A-Materials Science and Processing*, 63(2):109–115, 1996.

[9] T. B. Cox and J. R. Jr. Low. Investigation of the plastic fracture of aisi 4340 and 18 nickel em dash 200 grade maraging steels. *Metallurgical Transactions*, 5(6):1457–1470, 1974.

[10] J. Gammage, D. Wilkinson, Y. Brechet, and D. Embury. A model for damage coalescence in heterogeneous multi-phase materials. *Acta Materialia*, 52:52555263, 2004.

[11] A.L. Gurson. Continuum theory of ductile rupture by void nucleation and growth: Part 1 - yield criteria and flow rules for porous ductile media. *Journal of Engineering Materials and Technology*, 99, 1977.

[12] S. Jia and G.L. Povirk. Modeling the effects of hole distribution in perforated aluminum sheets ii: minimum strength failure paths. *International Journal of Solids and Structures*, 39:25332545, 2002.

[13] R. Le Harzic, N. Huot, E. Audouard, C. Jonin, P. Laporte, S. Valette, A. Fraczkiewicz, and R. Fortunier. Comparison of heat-affected zones due to nanosecond and femtosecond laser pulses using transmission electronic microscopy. *Applied Physics Letters*, 80(21):3886–3888, 2002.

[14] A. Luft, U. Franz, A. Emsermann, and J. Kaspar. A study of thermal and mechanical effects on materials induced by pulsed laser drilling. *Applied Physics A-Materials Science and Processing*, 63(2):93–101, 1996.

[15] P. E. Magnusen, E. M. Dubensky, and D. A. Koss. The effect of void arrays on void linking during ductile fracture. *Acta Metallurgica*, 36(6):1503–1509, 1988.

[16] F.A. McClintock. Criterion for ductile fracture by the growth of holes. *J. Appl. Mech.*, 35:363–371, 1968.

[17] S. Nagaki, Y. Nakayama, and T. Abe. Relation between damage due to circular holes and local deformation of perforated sheets. *International Journal of Mechanical Sciences*, 40(2-3):215–226, 1998.

[18] S. Nolte, C. Momma, G. Kamlage, A. Ostendorf, C. Fallnich, F. von Alvensleben, and H. Welling. Polarization effects in ultrashort-pulse laser drilling. *Applied Physics A: Materials Science and Processing*, 68(5):563–567, 1999.

[19] T. Pardoen and J.W. Hutchinson. An extended model for void growth and coalescence. *Journal of the Mechanics and Physics of Solids*, 48:24672512, 2000.

[20] J.R. Rice and D.M. Tracey. On the ductile enlargement of voids in triaxial stress fields. *Journal of the Mechanics and Physics of Solids*, 17:201–217, 1969.

[21] J. Thøgersen, A. Borowiec, H. K. Haugen, F. E. McNeill, and I. M. Stronach. X-ray emission from femtosecond laser micromachining. *Applied Physics A-Materials Science and Processing*, 73(3):361–363, 2001.

[22] P. F. Thomason. *Ductile Fracture of Metals*. Pergamon Press, Oxford, 1990.

[23] P.F. Thomason. A theory for ductile fracture by internal necking of cavities. *Journal of the Institute of Metals*, 96:360–365, 1968.

[24] K. Uesugi, Y. Suzuki, N. Yagi, A. Tsuchiyama, and T. Nakano. Development of high spatial resolution x-ray ct system at bl47xu in spring-8. *Nuclear Instruments and Methods in Physics Research Section A: Accelerators, Spectrometers, Detectors and Associated Equipment*, 467-468(Part 2):853–856, 2001.

[25] A. Weck, D. Wilkinson, H. Toda, and E. Maire. 2d and 3d visualization of ductile fracture. *Advanced Engineering Materials*, 8:469–472, 2006.

[26] A. E. Wynne and B. C. Stuart. Rate dependence of short-pulse laser ablation of metals in air and vacuum. *Applied Physics A-Materials Science and Processing*, 76(3):373–378, 2003.

[27] X. Zhu, D. M. Villeneuve, A. Yu. Naumov, S. Nikumb, and P. B. Corkum. Experimental study of drilling sub-10 μm holes in thin metal foils with femtosecond laser pulses. *Applied Surface Science*, 152:138–148, 1999.